An Analysis of the Size Selectivity of Solute Partitioning, Diffusion, and Permeation across Lipid Bilayers

Samir Mitragotri, Mark E. Johnson, Daniel Blankschtein, and Robert Langer
Department of Chemical Engineering, Massachusetts Institute of Technology, Cambridge, Massachusetts 02139 USA

ABSTRACT The lipid bilayers of cell membranes are primarily responsible for the low passive transport of nonelectrolytes across cell membranes, and for the pronounced size selectivity of such transport. The size selectivity of bilayer permeation has been hypothesized to originate from the hindered transport of solutes across the ordered-chain region. In this paper, we develop a theoretical description that provides analytical relationships between the permeation properties of the ordered-chain region of the lipid bilayer (partition and diffusion coefficients) and its structural properties, namely, lipid chain density, free area, and order parameter. Emphasis is placed on calculating the size selectivity of solute partitioning, diffusion, and overall permeability across the ordered-chain region of the lipid bilayer. The size selectivity of solute partitioning is evaluated using scaled-particle theory, which calculates the reversible work required to create a cavity to incorporate a spherical solute into the ordered-chain region of the lipid bilayer. Scaled-particle theory is also used to calculate the work required to create a diffusion path for solutes in the interfacial region of the lipid bilayer. The predicted size dependence of the bilayer permeability is comparable to that observed experimentally. The dependence of solute partition and diffusion coefficients on the bilayer structural parameters is also discussed.

INTRODUCTION

The barrier properties of biological membranes, such as the blood–brain barrier, the skin, and cell membranes, to solute transport arise from the remarkably low permeability of the lipid bilayers comprising these membranes (Stein, 1986). Several attempts have been made to develop relationships between the permeation properties of lipid bilayers, that is, solute partitioning and diffusion, and the physicochemical properties of the permeating solutes, such as size and lipophilicity (Leib and Stein, 1969; Xiang and Anderson, 1994a). Attempts have also been made to relate the transport properties of lipid bilayers to their structural properties, such as surface lipid density (Xiang and Anderson, 1997). Such relationships among solute permeability, bilayer structural parameters, and solute physicochemical parameters may potentially help in predicting the rates of drug delivery across membranes, as well as assist in the development of physicochemical enhancers capable of increasing membrane permeability. In spite of their potential value, such relationships are not available in the current literature.

Early studies aimed at developing structure–transport relationships were focused on relating solute partitioning into bilayers to that into simpler isotropic liquids, for example, octanol (Diamond and Katz, 1974; Johnson, 1996). These studies led to the development of phenomenological equations to predict bilayer partition coefficients using various solvents, including octanol, olive oil, hexadecane, and decadiene (Johnson, 1996; Diamond and Katz, 1974; Xiang and Anderson, 1994b). Although these equations have been successfully used in the analysis of transport properties of various membranes, experimental and theoretical analyses clearly show that solute partitioning into bilayers differs in many respects from that into bulk hydrocarbons. Specifically, the solute partition coefficient into bilayers exhibits a strong dependence on the local lipid microstructure, a feature that cannot be accounted for based on partition coefficients in bulk fluids (Marqusee and Dill, 1986; Xiang, 1993; Xiang and Anderson, 1993). The dependence of the partition coefficient on local lipid chain microstructure was demonstrated by the lattice calculations of Marqusee and Dill (1986), who showed that the highly-ordered structure of the lipid chains near the interface results in the steric expulsion of solutes from this region. As a result, solute partition coefficients into lipid bilayers exhibit spatial variations with a minimum near the interface and a maximum near the center of the bilayer. Experimental measurements of hexane partition coefficients have supported this hypothesis (White et al., 1981). More insight on solute partitioning into lipid bilayers has been gained through molecular dynamic (MD) simulations which have provided detailed information about the local microstructure within the bilayer (Xiang and Anderson, 1993; Marrink and Berendsen, 1994, 1996). These simulations confirmed that the ordered-chain region (a few-Å-thick region of highly-ordered lipid chains near the bilayer interface) results in the steric expulsion of solutes, and plays an important role in determining the overall permeability of lipid bilayers. Although the simulations have been helpful in understanding many aspects of bilayer solute permeation, the general dependence of bilayer permeability on the interfacial structure of the lipid bilayers is not yet well understood.

Attempts have also been made to develop analytical models to explain the size selectivity of bilayer permeation.

Received for publication 11 February 1999 and in final form 14 June 1999.
Address reprint requests to Dr. Samir Mitragotri, E25-342, MIT, 45 Carlton St., Cambridge, MA 02139. Tel.: 617-253-5359; Fax: 617-258-8827; E-mail: samir@mit.edu.
Mark E. Johnson's present address is Corixa Corporation, Seattle, WA.

0006-3495/99/09/1268/16 $2.00

Early models describing bilayer permeability attributed the entire size dependence of bilayer permeation to solute diffusion in the lipid bilayers and not to solute partitioning. Empirical equations relating diffusion coefficients to solute size were developed to explain the experimentally observed size selectivity of lipid bilayer permeation (Leib and Stein, 1969). However, recent MD simulations have shown that the size dependence of solute diffusion coefficients in bilayers, although stronger than that in an isotropic hydrocarbon, is weaker than that estimated using the empirical models (Marrink and Berendsen, 1996). In addition, the simulations also showed that the size dependence of lipid bilayer permeation may be attributed to both partitioning as well as diffusion in the ordered-chain region of the lipid bilayer, although their relative roles in determining the overall size selectivity are still unknown. Attempts have also been made to theoretically clarify the relative roles of partitioning and diffusion in determining size selectivity (Xiang, 1993), however, the quantitative dependence of the size selectivity of bilayer permeation on various bilayer parameters is not fully understood.

In this paper, we present a theoretical description that relates solute partition and diffusion coefficients to the solute size and to bilayer parameters, such as lipid density and CD-order parameter. The primary objective of this paper is to provide an analytical equation that allows prediction of bilayer permeability based on the experimentally measurable solute and bilayer parameters. The theoretical description is primarily based on scaled-particle theory, which relates the work required to create cavities in the lipid bilayer (to allow partitioning and diffusion of solutes) to lipid density, lipid order parameters, and solute radius. A comparison of the theoretical predictions with experimental results is also presented.

THEORY

The permeation resistance R of an isotropic membrane of thickness d to a solute is related to the solute diffusion coefficient D_o and the solute partition coefficient K_o as (Xiang and Anderson, 1997)

$$R = \frac{d}{D_o K_o}. \tag{1}$$

For a structurally-heterogeneous membrane, such as a bilayer, both the diffusion and the partition coefficients of the solute, and, hence, the permeation resistance, exhibit spatial variations. Furthermore, MD simulations of solute permeation have indicated that the maximum permeation resistance is typically offered by the ordered-chain region of the lipid bilayer (a few-Å-thick region of highly-ordered lipid chains near the bilayer interface) (Marrink and Berendsen, 1994, 1996). Experimental measurements of permeation resistance have also supported this hypothesis (Dix et al., 1978). In that case, Eq. 1 may be generalized to relate R to spatially-dependent solute diffusion and partition coefficients as

$$R = \frac{1}{P} = \int_o^{\delta} \frac{dz}{K_b(z) D_b(z)}, \tag{2}$$

where P is the lipid bilayer permeability, the suffix b denotes parameters corresponding to the bilayer ordered-chain region, z is the distance along the bilayer normal (perpendicular to the plane containing the lipid head groups), and δ is the ordered-chain region thickness. In the following sections, we describe the calculation of the solute partition coefficient $K_b(z)$ and diffusion coefficient $D_b(z)$.

Solute partition coefficient into the lipid ordered-chain region $K_b(z)$

The partition coefficient of a solute from an aqueous phase into a section of an ordered-chain region at a depth z, $K_b(z)$, can be described as

$$K_b(z) = \exp\left(\frac{-\Delta\mu_o(z)}{kT}\right), \tag{3}$$

where $\Delta\mu_o(z)$ is the change in the solute standard-state chemical potential associated with its transfer from the aqueous phase into the ordered-chain region at a depth z from the interface, k is the Boltzmann constant, and T is the absolute temperature. Xiang and Anderson (1993) have described the change in the solute standard-state chemical potential associated with solute transfer into bilayers as the sum of two contributions: the work required to create a cavity to incorporate the solute in the bilayer, and the change in the interactions of the solute with its surroundings, reflecting a change in the chemical microenvironment of the solute at a depth z. The standard-state chemical potential μ_o of a solute dissolved in a solvent may be described as

$$\mu_o = \mu_o^{ig} + W + \Delta\mu^{sur}, \tag{4}$$

where μ_o^{ig} is the solute standard-state chemical potential in an ideal-gas reference state, W is the reversible work required to create a cavity in the solvent to incorporate the solute from the ideal-gas state, and $\Delta\mu^{sur}$ is the change in the solute standard-state chemical potential during its transfer from the ideal-gas state to the solvent due to changes in its interactions with the surroundings. Note that $\Delta\mu^{sur}$ depends on the nature, as well as on the range, of the solute interactions with its surroundings. Accordingly, $\Delta\mu^{sur}$ may also depend on the location (depth) of the solute in the bilayer. Using Eq. 4 to describe solute partitioning from water into a bilayer at a depth z, one obtains

$$\Delta\mu_o(z) = W_b(z) - W_a + \Delta\mu_{a-b}^{sur}(z), \tag{5}$$

where $W_b(z)$ is the reversible work required to create a cavity to incorporate the solute in the bilayer at a depth z, W_a is the reversible work required to create a cavity to incor-

porate the solute in the aqueous environment, and $\Delta\mu^{sur}_{a-b}(z)$ is the change in the solute standard-state chemical potential due to changes in its microenvironment during the transfer from water into the bilayer at a depth z. Using Eq. 5 in Eq. 3, one obtains

$$K_b(z) = \exp\left(\frac{-W_b(z) - \Delta\mu^{sur}_{a-b}(z) + W_a}{kT}\right). \quad (6)$$

To compare solute partition coefficients from water into bilayers with those from water into isotropic solvents, an expression similar to Eq. 6 can be derived to describe solute partitioning from water into an isotropic solvent. Specifically,

$$K_o = \exp\left(\frac{-W_o - \Delta\mu^{sur}_{a-o} + W_a}{kT}\right), \quad (7)$$

where W_o is the reversible work required to create a cavity to incorporate the solute in the isotropic solvent, and $\Delta\mu^{sur}_{a-o}$ is the change in the solute standard-state chemical potential due to changes in its microenvironment during the transfer from water to the isotropic solvent. Several attempts have been made to identify solvents that mimic the chemical microenvironment in the lipid bilayer (Johnson, 1996; Diamond and Katz, 1974; Xiang and Anderson, 1994b). Examples of these solvents include octanol, decadiene, hexadecane, and olive oil. It is unlikely that a single solvent can accurately represent the local chemical microenvironment in the entire ordered-chain region. However, for simplicity, we assume that $\Delta\mu^{sur}_{a-b}(z)$ is relatively insensitive to the precise location in the ordered-chain region, and therefore, can be represented by that corresponding to a single solvent that mimics the average chemical microenvironment of the ordered-chain region. Although this assumption oversimplifies the chemical microenvironment in the ordered-chain region, we will show that it is a reasonable assumption that facilitates the evaluation of the size selectivity of bilayer permeation. Assuming that $\Delta\mu^{sur}_{a-b}(z)$ is comparable to $\Delta\mu^{sur}_{a-o}$ and combining Eqs. 6 and 7, one obtains (Xiang, 1993)

$$K_b(z) = K_o\exp\left(\frac{-W_b(z) + W_o}{kT}\right). \quad (8)$$

Numerous theoretical calculations, as well as simulations, have been performed to evaluate the work of cavity formation in isotropic fluids, W_o (Helfand et al., 1961; Hummer et al., 1996). In contrast, in the case of lipid bilayers, such calculations rely primarily on simulations (Xiang, 1993; Marrink and Berendsen, 1996). Our emphasis in this paper is on developing analytical equations that relate $W_b(z)$ to the physical properties of the lipid bilayer, including lipid chain density and CD-order parameter, using scaled-particle theory as described below. To highlight the fact that $W_b(z)$, W_o, $K_b(z)$, and K_o all depend on solute radius, r, hereafter, we denote these as $W_b(r, z)$, $W_o(r)$, $K_b(r, z)$, and $K_o(r)$, respectively.

Calculation of $W_b(r, z)$

The work required to introduce a spherical solute of radius, r, into the ordered-chain region can be estimated using a two-dimensional (2D) model of the lipid chains. Underlying such a model is the assumption that the work required to create a cavity to incorporate the solute is due solely to the lateral (2D) expansion of the bilayer against the lateral pressure generated by the lipid chains. This assumption is reasonable for solute partitioning into the ordered-chain region because the lipid chains in this region are highly ordered and densely packed. Accordingly, the lateral displacement of the lipid chains is likely to be geometrically (and hence energetically) more favorable compared to any other displacement modes. For the purpose of calculating $W_b(r, z)$ in the ordered-chain region, the lipid chains are modeled as a series of connected cylinders each having a hard-core radius R and length l (approximately equal to the length of a C–C bond) (see Fig. 1 *A*). Hence, the number of rods comprising the lipid chain is equal to the number of C–C bonds in the lipid tail. As will be shown later, the lipid head group does not enter into the calculations. The cylinder

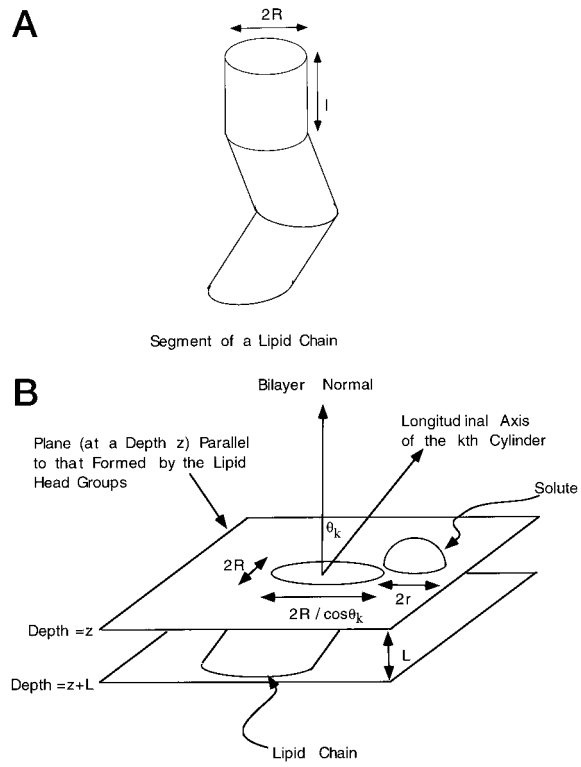

FIGURE 1 (*A*) Model lipid chain used in our study, showing three C–C segments, each modeled as a cylinder of radius R and length l. (*B*) Section of a lipid chain oriented at an angle θ_κ (with respect to the bilayer normal), which is located between depths z and $z + L$. Also shown is a cross section of this lipid chain on a plane located at z parallel to the lipid head groups. The cross section of the lipid cylinder is an ellipse with a major axis $R/\cos\theta_\kappa$ and a minor axis R. Also shown is a solute having a radius r ($r < L$) located next to the lipid chain. The cross section of the solute in the plane located at z parallel to that formed by the lipid head groups is a circle with a radius r.

describing a C–C bond is designed around it such that the longitudinal axis of the cylinder coincides with the normal to the plane containing the CH_2 bonds (Salmon et al., 1987). The angle between the longitudinal axis of the kth cylinder and the bilayer normal is denoted by θ_κ ($0 \le \theta_k \le \pi/2$), and varies from cylinder to cylinder. Consider a section of lipid chains having an area A and thickness L at a depth z, as shown in Fig. 1 *B*. Figure 1 *B* also shows a solute of radius r next to a lipid chain. Consider the cross-section of the lipid chain in a plane parallel to that formed by the head groups located at a depth z. In this projection, let s_k denote the fraction of cylinders making an angle θ_κ with the bilayer normal. Accordingly, this cross-section contains Ns_k ellipses, each having a major axis, $R/\cos\theta_k$, and a minor axis, R (see Fig. 1 *B*), where N is the total number of disks in the area A (that is, the disk density is $\rho = N/A$). With this description of the lipid chains, the work $W_b(r, z)$ required to create a cavity to accommodate a solute of radius r can be calculated using scaled-particle theory (see the Appendix). The resulting expression is given by

$$\beta W_b(r, z) = -\ln(a_f) + \frac{2(1 - a_f)\xi}{a_f\psi(1 + \psi)}\left(\frac{r}{R}\right) + \frac{1}{\psi}\left(\frac{1 - \xi/\psi}{a_f} + \frac{\xi}{2\psi a_f^2} + \frac{\xi}{2\psi} - 1\right)\left(\frac{r}{R}\right)^2, \quad (9)$$

where $\beta = 1/kT$, a_f is the free area per lipid molecule at z and is given by

$$a_f = 1 - \pi R^2\rho\psi, \qquad \psi = \sum_{k=1}^{N} \frac{s_k}{\cos\theta_k},$$

and

$$\xi = (1 + \psi)\sum_{k=1}^{N} s_k\sqrt{\frac{1}{2}\left(1 + \frac{1}{\cos^2\theta_k}\right)}.$$

Strictly speaking, Eq. 9 is only applicable in cases where considerations of only a single layer of lipid segments is required, that is, when the solute radius r is smaller than the length of the lipid segment, $l \sim 1.54$ Å. This follows from the fact that if $r > l$, then structural parameters (density and orientation) of the adjacent lipid segment also need to be considered in the calculations (see also the Appendix). However, as will be shown later, Eq. 9 still provides a reasonable estimate of the work of cavity formation for solutes having a radius greater than ~1.54 Å. To actually use Eq. 9, ψ and ξ must be evaluated in terms of the measurable lipid order parameters. The most commonly used lipid order parameter is the CD-order parameter, S_{CD}, given by $S_{CD} = \langle P_2(\cos\beta_{PD})\rangle$, where β_{PD} is the angle between the C–H bond vector (that is, the normal to the plane defined by the C–H bonds) and the bilayer normal (Jansson et al., 1992), P_2 is the second-order Legendre polynomial, and the averaging is performed over all lipid chains having a certain segmental position. The angle θ_κ of the lipid chains may be related to β_{PD} through the tetrahedral geometry of the C–C bonds in a lipid chain. As a first step in relating ψ to S_{CD}, ψ was expanded in a Taylor series in $\cos\theta_\kappa$ around $\theta_\kappa = 0$ (truncated after the first term in $\cos\theta_\kappa$), and averaged, term by term, over all chain orientations to obtain the approximate expression

$$\psi \approx 2 - \langle\cos\theta_k\rangle. \quad (10)$$

Following similar steps, ξ was found to be

$$\xi \approx \sqrt{\psi}(1 + \psi). \quad (11)$$

The quantity $\langle\cos\theta_k\rangle$ can, in turn, be related to S_{CD} as (Jansson et al., 1992)

$$\langle\cos\theta_k\rangle = \tfrac{1}{2} - S_{CD}. \quad (12)$$

Therefore, Eqs. 10 and 11 can be rewritten, respectively, as

$$\psi \approx \tfrac{3}{2} + S_{CD}, \quad (13)$$

$$\xi \approx (\tfrac{3}{2} + S_{CD})^{1/2}(\tfrac{5}{2} + S_{CD}). \quad (14)$$

Eq. 9, in combination with Eqs. 13 and 14, allows the prediction of the work required to introduce a circular cavity (corresponding to the cross-section of a spherical solute) into a plane located in the ordered-chain region at a depth z from the bilayer surface.

Calculation of $W_o(r)$

The lipid chains in an isotropic solvent (for example, octanol) are more disordered, and, therefore, may displace in all three dimensions to accommodate the partitioning solute. Hence, the work of cavity formation, $W_o(r)$, required to introduce a solute into an isotropic solvent needs to be estimated using a three-dimensional (3D) model. Cavity formation in isotropic solvents has been studied extensively using simulations as well as a combination of simulations and theoretical approaches (Hummer et al., 1996). To be consistent with our previous analysis of the lipid chains in a bilayer, we will use a simple hard-sphere model to calculate the work of cavity formation in liquids using scaled-particle theory (Helfand et al., 1961; Reiss et al., 1959). The work $W_o(r)$ required to insert a spherical solute of radius r into the isotropic solvent, modeled as a collection of hard spheres of radius R_h can be described as (Lebowitz et al., 1965)

$$\beta W_o(r) = -\ln(v_f) + \frac{3(1 - v_f)}{v_f}\left(\frac{r}{R_h}\right) + \left(\frac{3(1 - v_f)}{v_f} + \frac{9(1 - v_f)^2}{2v_f^2}\right)\left(\frac{r}{R_h}\right)^2 + \beta\frac{4}{3}\pi r^3 P, \quad (15)$$

where v_f is the fraction of free volume ($v_f = 1 - 4\pi R_h^3\rho_h/3$), ρ_h is the hard-sphere density, and P is the pressure. Eq. 15 is derived by combining Eqs. 2.7 and 2.8 of Lebowitz et al. (1965), and then applying the resulting equation to a single-

component system. Under normal pressures (~1 atmosphere), the contribution of the last term in Eq. 15 is negligible for cavities considered in this study ($r < 4$ Å), and, hence, it is excluded in all further equations. Eq. 15 is a 3D-equivalent of Eq. 9. This analogy is clear from a comparison of the coefficients of the r^0, r^1, and r^2 terms in Eqs. 9 and 15. For example, the coefficient of r^1, $3(1 - v_f)/v_f$, in Eq. 15 is analogous to the coefficient of r^1, $2(1 - a_f)\xi/a_f\psi(1 + \psi)$, in Eq. 9. The analogy is even clearer if the lipid chains were aligned along the bilayer normal (in that case, $\theta_k = 0$, which yields $\psi = 1$ and $\xi = 2$), for which the coefficient of r^1 in Eq. 9 becomes $2(1 - a_f)/a_f$, which is similar to the r^1 term in Eq. 15. The parameter v_f in Eq. 15 is analogous to the parameter a_f in Eq. 9 and the factors 3 and 2, respectively, indicate the dimensionality of Eqs. 15 and 9. Note that the pressure–volume term in Eq. 15 does not appear in Eq. 9 because this equation describes a 2D system.

Calculation of $K_b(r, z)/K_o(r)$

It is now possible to calculate the solute partition coefficient in the ordered-chain region of the lipid bilayer relative to that in an isotropic solvent using Eqs. 8, 9, and 15. Specifically,

$$\frac{K_b(r, z)}{K_o(r)} = \exp(A + Br + Cr^2), \tag{16}$$

where

$$A = \ln\left(\frac{a_f}{v_f}\right), \qquad B = \left(\frac{3(1 - v_f)}{v_f R_h} - \frac{(1 - a_f)2\xi}{a_f\psi(1 + \psi)R}\right),$$

and

$$C = \left(\frac{3(1 - v_f)}{v_f R_h^2} + \frac{9(1 - v_f)^2}{2v_f^2 R_h^2} - \frac{1 - \xi/\psi}{\psi a_f R^2} - \frac{\xi}{2\psi^2 a_f^2 R^2} - \frac{\xi}{2\psi^2 R^2} + \frac{1}{\psi R^2}\right).$$

Eq. 16, along with Eqs. 13 and 14, relates the relative partition coefficient of a solute of radius r at a given depth z in the ordered-chain region $K_b(r, z)/K_o(r)$ to the free area per lipid chain a_f, the CD-order parameter S_{CD}, the lipid chain radius R, the fraction of free volume in the model isotropic solvent v_f, and the hard-sphere radius of a solvent molecule R_h. Eq. 16 is discussed further in the Results and Discussion section.

Solute diffusion across the ordered-chain region $D_b(r, z)$

Solute diffusion in lipid bilayers has been described in terms of hops between free-volume pockets (Vaz et al., 1985; Vaz and Almeida, 1991). The solute is assumed to rattle in a free-volume pocket until it finds another large pocket to jump into. The solute diffusion coefficient then simply depends on the availability of a free-volume pocket into which the solute can jump. In our approach, we assume that a spherical solute of radius r can move through a distance ϵ at an angle ω with respect to the bilayer normal only if a continuous spherocylindrical path of length ϵ is free of the solvent molecules, that is, if a spherocylindrical free-volume pocket of radius r and length ϵ exists (see Fig. 2 *A*) in that direction. A similar approach has been used by Han and Herzfeld (1993) to describe diffusion in crowded protein solutions and by Xiang (1999) to describe diffusion in lipid bilayers. The diffusion coefficient of a spherical solute of radius r along the bilayer normal, (corresponding to $\omega = 0$), can then be written as

$$D(r) = D^*(r)\int_{\epsilon^*}^{\infty} [p_\perp(r, \epsilon) \cap P(r)]\, d\epsilon, \tag{17}$$

where $D^*(r)$ is the solute diffusion coefficient within a free-volume pocket, $p_\perp(r, \epsilon) \cap P(r)\, d\epsilon$ is the conditional probability density that a spherocylindrical path of radius r and length between ϵ and $\epsilon + d\epsilon$ exists in the direction of diffusion (in our case, in the direction along the bilayer normal), and ϵ^* is the critical path length required for solute diffusion. The parameter ϵ^* denotes the critical length through which the solute must traverse for it to be displaced across the entire interfacial region. The parameter ϵ^* accounts for the fact that, if the solute displacement is too small, the solute may not move substantially over a large length scale. In other words, a certain critical displacement is required to achieve measurable diffusion. This issue is further discussed in the section, Estimation of Model Parameters.

The conditional probability density, $p_\perp(r, \epsilon) \cap P(r)\, d\epsilon$, can be related to the work required to create a spherocylindrical cavity of radius r and length ϵ in the ordered-chain region based on scaled-particle theory (Han and Herzfeld, 1993). Specifically,

$$\left[\int_{\epsilon^*}^{\infty} p_\perp(r, \epsilon) \cap P(r)\, d\epsilon\right]_{\text{bilayer}} = \exp\{-\beta[W_b^d(r, \epsilon^*, z) - W_b(r, z)]\}, \tag{18}$$

where $W_b(r, z)$ is the work required to create a circular cavity of radius r (corresponding to a cross-section of a spherical solute on the plane parallel to that formed by the lipid head groups) at a depth z in the bilayer (given in Eq. 9), and $W_b^d(r, \epsilon^*, z)$ is the work required to create a cavity of radius r and length ϵ^* in a direction normal to the bilayer plane beginning at a depth z. Eq. 18 thus relates the solute diffusion coefficient to the geometric parameters character-

izing the solute and the lipid chains. Similarly, the probability of cavity formation for solute diffusion in an isotropic liquid is given by

$$\left[\int_{\epsilon^*}^{\infty} p_{\perp}(r, \epsilon) \cap P(r)\, d\epsilon\right]_{\text{isotropic}} = \exp\{-\beta[W_o^d(r, \epsilon^*) - W_o(r)]\}, \quad (19)$$

where $W_o(r)$ is the work required to create a spherical cavity of radius r in the isotropic liquid (given in Eq. 15), and $W_o^d(r, \epsilon^*)$ is the work required to create a cavity of radius r and length ϵ^* in the same isotropic solvent in any direction. The ratio of the diffusion coefficients in the bilayer and in the isotropic liquid, $D_b(r, z)/D_o(r)$, can now be calculated using Eqs. 17, 18, and 19 as

$$\frac{D_b(r, z)}{D_o(r)} = \exp[-\beta\{W_b^d(r, \epsilon^*, z) - W_b(r, z) - W_o^d(r, \epsilon^*) + W_o(r)\}]. \quad (20)$$

The calculations of $W_b(r, z)$ and $W_o(r)$ have already been described in the previous section (see Eqs. 9 and 15, respectively). Below, we describe the calculations of $W_b^d(r, \epsilon^*, z)$ and $W_o^d(r, \epsilon^*)$.

Calculation of $W_b^d(r, \epsilon^*, z)$

Figure 2 *B* shows a section of a lipid chain oriented at an angle θ_k with respect to the bilayer normal and a solute of radius r diffusing along the normal. The work required to create a spherocylindrical cavity of radius r and length ϵ along the normal is related to the excluded volume between the solute spherocylinder and the lipid chain. Because, as shown earlier, the lipid chains near the interfacial region are modeled as a 2D fluid that can only expand laterally, the work of cavity formation is equal to that required to create a circular cavity in an elliptical hard-disk fluid with major axis $R/\cos\theta_k + \epsilon \tan\theta_k$ and minor axis R (see Fig. 2 *B*). The work of cavity formation $W_b^d(r, \epsilon^*, z)$ can then be calculated using the approach presented in the Appendix, which was used to arrive at Eq. 9. The resulting equation is identical to Eq. 9 except that the term $1/\cos\theta_k$ in Eq. 9 is replaced by $1/\cos\theta_k + (\epsilon^*/2R)\tan\theta_k$. The resulting equation is

$$\beta W_b^d(r, \epsilon^*, z) = -\ln(\kappa) + \frac{2(1-\kappa)\chi}{\kappa\phi(1+\phi)}\left(\frac{r}{R}\right) + \frac{1}{\phi}\left(\frac{1-\chi/\phi}{\kappa} + \frac{\chi/2\phi}{\kappa^2} + \frac{\chi}{2\phi} - 1\right)\left(\frac{r}{R}\right)^2, \quad (21)$$

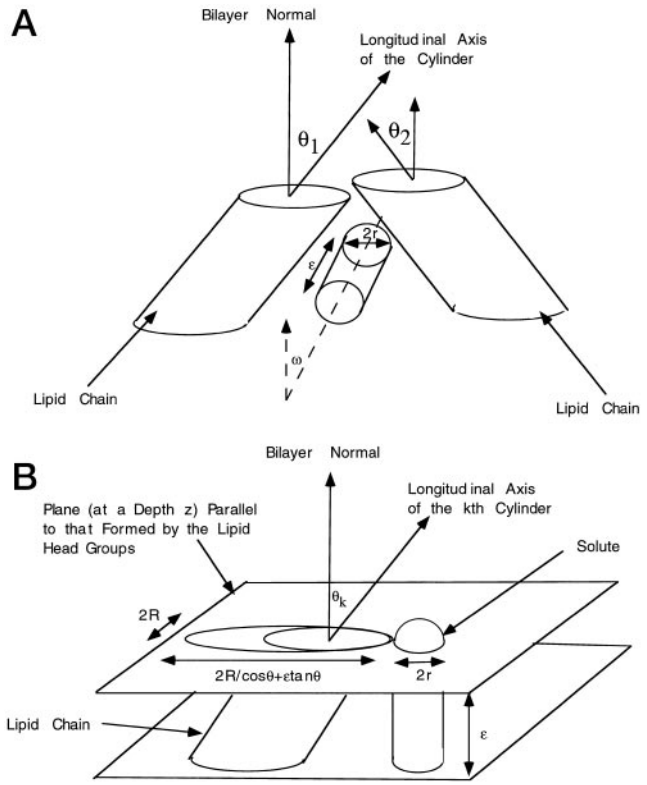

FIGURE 2 (*A*) A schematic representation of a solute of radius r displacing through a distance ϵ within lipid chains oriented at an angle ω with respect to the bilayer normal. Two lipid chains oriented at angles θ_1 and θ_2 with respect to the bilayer normal are shown. The solute can displace through a distance ϵ only if a continuous spherocylindrical path, as shown, is free of lipid chains. (*B*) A projection of a solute of radius r diffusing along the bilayer normal ($\omega = 0$) through a distance ϵ next to a lipid cylinder oriented at an angle θ_k with respect to the bilayer normal. The projection of the lipid chain on the plane at z is an ellipse with a major axis $2R/\cos\theta + \epsilon \tan\theta$ and a minor axis R.

where

$$\phi = \sum_{k=1}^{N} s_k\left(\frac{1}{\cos\theta_k} + \frac{\epsilon^*}{2R}\tan\theta_k\right),$$

$$\chi = (1+\phi)\sum_{k=1}^{N} s_k\sqrt{\frac{1}{2}\left(1 + \left(\frac{1}{\cos\theta_k} + \frac{\epsilon^*}{2R}\tan\theta_k\right)^2\right)},$$

$\kappa = (1 - \pi R^2\rho\phi)$, N is the number of disks, and ρ ($= N/A$) is the disk number density. Eq. 21 relates the work required to create a diffusion path within the lipid chains to bilayer parameters, including chain (or disk) density ρ, chain radius R, and average chain orientation, as well as to solute parameters, including its radius r and critical diffusion path length ϵ^*. The analogy between Eqs. 9 and 21 is quite apparent. The parameters κ, ϕ, and χ in Eq. 21, correspond, respectively, to the parameters a_f, ψ, and ξ in Eq. 9, and they become equal when $\epsilon^* = 0$. To calculate $W_b(r, \epsilon^*, z)$, ϕ and χ must be evaluated in terms of the experimentally measur-

able order parameter S_{CD} in a manner similar to that described above. Specifically,

$$\phi = \psi + \frac{\epsilon^*}{2R}\langle \tan \theta_k \rangle \tag{22}$$

and

$$\chi = \sqrt{\phi}(1 + \phi). \tag{23}$$

Eqs. 22 and 23 are similar to Eqs. 10 and 11, respectively, and they become equal when $\epsilon^* = 0$. Because the values of θ_k in the interfacial region are relatively small (average value of about 30–35° (Huang et al., 1994)), $\langle \tan \theta_k \rangle$ may be approximated by $\tan\langle \theta_k \rangle$. To test the error introduced by this approximation, we generated one thousand values of θ_k randomly distributed between 0 and 30°. In that case, $\tan\langle \theta_k \rangle$ is within 4% of $\langle \tan \theta_k \rangle$. For the same reason, assuming that $\langle \cos \theta_k \rangle \approx \cos\langle \theta_k \rangle$ in Eq. 12 yields $\langle \theta_k \rangle \approx \cos^{-1}(\frac{1}{2} - S_{CD})$. Using this result, it follows that

$$\langle \tan \theta_k \rangle \approx \tan\langle \theta_k \rangle = \tan(\cos^{-1}(\tfrac{1}{2} - S_{CD})). \tag{24}$$

Eqs. 22–24 can then be substituted in Eq. 21 to calculate $W_b^d(r, \epsilon^*, z)$.

Calculation of $W_o^d(r, \epsilon^*)$

Cotter (1977) has described the calculation of the work of cavity formation in a solvent consisting of spherocylindrical molecules. That analysis can be modified to calculate the work required to create spherocylindrical cavities of radius r and length ϵ^* in a hard-sphere liquid to arrive at the equation

$$\begin{aligned}\beta W_o^d(r, \epsilon^*) = &-\ln(v_f) + \frac{3(1 - v_f)}{v_f}\left(\frac{r}{R_h}\right) + \frac{3(1 - v_f)}{4v_f}\left(\frac{\epsilon^*}{R_h}\right) \\ &+ \left(\frac{3(1 - v_f)}{v_f} + \frac{9(1 - v_f)^2}{2v_f^2}\right)\left(\frac{r^2}{R_h^2} + \frac{r\epsilon^*}{2R_h^2}\right) \\ &+ \beta\left(\frac{4}{3}\pi r^3 + \pi r^2 \epsilon^*\right)P.\end{aligned} \tag{25}$$

Eq. 25 is very similar to Eq. 15, except for the presence of two additional terms that are linear in ϵ^* (due to the linear increase of the cavity volume with ϵ^*). Once again, for small cavities ($r < 4$ Å), the contribution of the last term (the pressure–volume term) in Eq. 25 may be neglected.

Calculation of $D_b(r, z)/D_o(r)$

It is now possible to calculate the ratio of diffusion coefficients, $D_b(r, z)/D_o(r)$, by using Eqs. 9, 21, 25, and 15 in Eq. 20. Specifically,

$$\frac{D_b(r, z)}{D_o(r)} = \exp(A' + B'r + C'r^2 + D'\epsilon^*), \tag{26}$$

where

$$A' = \ln\left(\frac{\kappa}{a_f}\right), \qquad B' = \frac{(1 - \kappa)2\chi}{\kappa\phi(1 + \phi)R} - \frac{(1 - a_f)2\xi}{a_f\psi(1 + \psi)R},$$

$$\begin{aligned}C' = &\frac{1}{\phi R^2}\left(\frac{1 - \chi/\phi}{\kappa} + \frac{\chi/2\phi}{\kappa^2} + \frac{\chi}{2\phi} - 1\right) \\ &- \frac{1}{\psi R^2}\left(\frac{1 - \xi/\psi}{a_f} + \frac{\xi/2\psi}{a_f^2} + \frac{\xi}{2\psi} - 1\right),\end{aligned}$$

and

$$D' = -\frac{3(1 - v_f)}{4v_f R_h} - \left(\frac{3(1 - v_f)}{2v_f} + \frac{9(1 - v_f)^2}{4v_f^2}\right)\frac{r}{R_h^2}.$$

Eq. 26 indicates that the relative solute diffusion coefficient in the lipid bilayer, $D_b(r, z)/D_o(r)$, depends on the free area per lipid chain a_f, the CD-order parameter S_{CD}, the lipid chain radius R, the fraction of free volume in the model isotropic solvent v_f, the solvent particle radius R_h, and the critical path for solute diffusion ϵ^*. Eq. 26 is discussed further in the Results and Discussion section.

Solute permeation across the lipid bilayer interface

The permeability $P_b(r)$, across the ordered-chain region of the lipid bilayer, and hence approximately across the entire lipid bilayer, relative to the permeability $P_o(r)$ of a film of an isotropic fluid of the same thickness δ, can now be evaluated using Eqs. 2, 8, and 20. Specifically,

$$\begin{aligned}\frac{P_o(r)}{P_b(r)} &= \frac{1}{\delta}\int_0^\delta \frac{D_o(r)}{D_b(r, z)}\frac{K_o(r)}{K_b(r, z)}\,dz \\ &= \frac{\exp[-\beta W_o^d(r, \epsilon^*)]}{\delta}\int_0^\delta \exp[\beta W_b^d(r, \epsilon^*, z)]\,dz.\end{aligned} \tag{27}$$

To solve Eq. 27, the evaluation of $W_b^d(r, \epsilon^*, z)$ at various depths z is required. This, in turn, requires knowledge of the z-dependencies of the lipid density ρ and of the CD-order parameter S_{CD} (see Eq. 9). Although the z-dependence of S_{CD} has been measured experimentally (Seeling and Seeling, 1974), as well as evaluated through simulations (Xiang, 1993), the z-dependence of ρ can only be obtained by simulations (Marrink and Berendsen, 1996). These values of ρ and S_{CD} could then be used to numerically evaluate Eq. 27. However, our main objective in this paper is to arrive at analytical relationships that allow calculation of $P_b(r)/P_o(r)$ entirely based on the experimentally-measurable bilayer parameters. For this purpose, we propose the following approximations to calculate $W_b^d(r, \epsilon^*, z)$.

Eq. 21, which relates $W_b^d(r, \epsilon^*, z)$ to the lipid density ρ and the chain orientations θ_κ, can be rewritten, after substituting $\chi = \sqrt{\phi}(1 + \phi)$ from Eq. 23 as

$$\beta W_b^d(r, \epsilon^*, z) = -\ln(\kappa) + \frac{2(1-\kappa)}{\kappa}\left(\frac{r}{R\sqrt{\phi}}\right) + \left(\frac{1-\alpha}{\kappa} + \frac{\alpha}{2\kappa^2} + \frac{\alpha}{2} - 1\right)\left(\frac{r}{R\sqrt{\phi}}\right)^2, \quad (28)$$

where $\alpha = (1 + \phi)/\sqrt{\phi}$. Note that κ depends on ρ as well as on S_{CD}. We now assume that the average lipid density in the ordered-chain region is equal to the surface lipid density σ (that is, to $\sigma = \rho_{z=0}$), a parameter that can be measured experimentally. In addition, molecular simulations have shown that, although the CD-order parameter exhibits strong variations with depth z, it plateaus near the interfacial region at a value denoted by $S_{CD}^{plateau}$. Hence, we assume that the average CD-order parameter in the interfacial region can be represented by $S_{CD}^{plateau}$. A typical value of $S_{CD}^{plateau}$ for dipalmitoyl phosphatidyl choline (DPPC) bilayers is -0.2 (Seeling and Seeling, 1974) corresponding to an average chain tilt angle of about 45°. As we will show later, Eq. 28, after modifications corresponding to these assumptions, provides an accurate description of the work of cavity formation in the ordered-chain region. Substituting this value into Eqs. 22–24, and evaluating κ (with a typical value of $\epsilon^* = 1.1$ Å [see Estimation of Model Parameters] and $R = 2.48$ Å [see Estimation of Model Parameters]) yields $\alpha = 2.04$. By taking $\alpha = 2$, Eq. 28 can now be simplified as

$$\langle \beta W_b^d(r, \epsilon^*)\rangle_{int} = -\ln(\kappa_{int}) + 2\left(\frac{1-\kappa_{int}}{\kappa_{int}}\right)\frac{r}{R^*} + \left(\frac{1}{\kappa_{int}^2} - \frac{1}{\kappa_{int}}\right)\left(\frac{r}{R^*}\right)^2, \quad (29)$$

where $\langle \beta W_b^d(r, \epsilon^*\rangle_{int}$ is the average work of cavity formation in the ordered-chain region, $R^* = R\sqrt{\phi^{plateau}}$, $\phi^{plateau}$ is the ϕ value calculated using $S_{CD} = S_{CD}^{plateau}$, and κ_{int} is the value of κ in the ordered-chain region. By substituting $\kappa_{int} = (1 - \sigma a_h \Gamma)$, where σ is the surface lipid density, $a_h = \pi R^2 \psi^{plateau}$ = the cross sectional area of a lipid chain (the minimum area occupied by a lipid chain at the surface), and $\Gamma = \phi^{plateau}/\psi^{plateau}$, where $\psi^{plateau}$ is the ψ value calculated using $S_{CD} = S_{CD}^{plateau}$, Eq. 29 can be rewritten as

$$\langle \beta W_b^d(r, \epsilon^*)\rangle_{int} = -\ln(1 - \sigma a_h \Gamma) + 2\left(\frac{\sigma\sqrt{\pi a_h \Gamma}}{1 - \sigma a_h \Gamma}\right)r + \left(\frac{\sigma\pi}{(1 - \sigma a_h \Gamma)^2}\right)r^2 \quad (30)$$

where

$$\Gamma = \frac{\phi^{plateau}}{\psi^{plateau}} = 1 + \frac{\epsilon^*}{2R}\left(\frac{\tan\cos^{-1}(\tfrac{1}{2} - S_{CD}^{plateau})}{(\tfrac{3}{2} + S_{CD}^{plateau})}\right).$$

Note that Γ contains the entire ϵ^* dependence of Eq. 30. Note also that when $\epsilon^* = 0$, Γ is equal to 1. Eq. 30 is expressed solely in terms of three bilayer parameters, σ, a_h, and $S_{CD}^{plateau}$, all of which can be measured experimentally (White and King, 1985; Kumar, 1991). Numerous measurements exist in the literature for these three parameters (White and King, 1985; Kumar, 1991; Seeling and Seeling, 1974). For example, DPPC bilayers are characterized by $\sigma \sim 0.033$ chains/Å^2 (Seeling and Seeling, 1974; Xiang, 1993) and $a_h \sim 20.4$ Å^2/chain (Xiang and Anderson, 1997). Substituting Eq. 30 in Eq. 27, the permeability $P_b(r)$, across the ordered-chain region of the lipid bilayer (denoted hereafter as $P_b^{int}(r)$ to emphasize the averaging performed in the ordered-chain region, as shown in Eq. 29), relative to the permeability $P_o(r)$ of a film of an isotropic fluid of the same thickness δ, can be written as

$$\frac{P_b^{int}(r)}{P_o(r)} = \exp\left[\ln(1 - \sigma a_h \Gamma) - 2\left(\frac{\sigma\sqrt{\pi a_h \Gamma}}{1 - \sigma a_h \Gamma}\right)r - \left(\frac{\sigma\pi}{(1 - \sigma a_h \Gamma)^2}\right)r^2\right] \div \left\{\exp\left[\ln(\nu_f) - \frac{3(1-\nu_f)}{\nu_f}\left(\frac{r}{R_h}\right) - \frac{3(1-\nu_f)}{4\nu_f}\left(\frac{\epsilon^*}{R_h}\right) - \left(\frac{3(1-\nu_f)}{\nu_f} + \frac{9(1-\nu_f)^2}{2\nu_f^2}\right)\left(\frac{r^2}{R_h^2} + \frac{r\epsilon^*}{2R_h^2}\right)\right]\right\}. \quad (31)$$

Because interfacial transport is the rate-limiting step in trans-bilayer transport, the interfacial permeability $P_b^{int}(r)$ should approximately represent the solute bilayer permeability. Following similar steps, the interfacial partition coefficient $K_b^{int}(r)$ relative to that in an isotropic solvent $K_0(r)$ (given in Eq. 8) can be written as

$$\frac{K_b^{int}(r)}{K_o(r)} = \exp\left[\ln(1 - \sigma a_h) - 2\left(\frac{\sigma\sqrt{\pi a_h}}{1 - \sigma a_h}\right)r - \left(\frac{\sigma\pi}{(1 - \sigma a_h)^2}\right)r^2\right] \div \left\{\exp\left[\ln(\nu_f) - \frac{3(1-\nu_f)}{\nu_f}\left(\frac{r}{R_h}\right) - \left(\frac{3(1-\nu_f)}{\nu_f} + \frac{9(1-\nu_f)^2}{2\nu_f^2}\right)\left(\frac{r}{R_h}\right)^2\right]\right\}. \quad (32)$$

Note that the interfacial partition coefficient of the lipid bilayer is not to be confused with the overall bilayer partition coefficient that is measured experimentally. The overall bilayer partition coefficient is much higher than the ordered-chain partition coefficient due to the higher free volume fraction near the center of the bilayer into which the solute can partition. Finally, using an approach similar to that used to arrive at Eq. 31, an expression for the diffusion coefficient in the ordered-chain region $D_b^{int}(r)$, relative to that in an isotropic solvent $D_o(r)$ (given in Eq. 20), can also be

derived

$$\frac{D_b^{int}(r)}{D_o(r)} = \exp\left[\ln\left(\frac{1-\sigma a_h\Gamma}{1-\sigma a_h}\right) - 2\left(\frac{\sigma\sqrt{\pi a_h\Gamma}}{1-\sigma a_h\Gamma} - \frac{\sigma\sqrt{\pi a_h}}{1-\sigma a_h}\right)r - \left(\frac{\sigma\pi}{(1-\sigma a_h\Gamma)^2} - \frac{\sigma\pi}{(1-\sigma a_h)^2}\right)r^2\right] \div\left\{\exp\left[-\frac{3(1-v_f)}{4v_f}\left(\frac{\epsilon^*}{R_h}\right) - \left(\frac{3(1-v_f)}{v_f} + \frac{9(1-v_f)^2}{2v_f^2}\right)\left(\frac{r\epsilon^*}{2R_h^2}\right)\right]\right\}. \quad (33)$$

Eqs. 31–33 are the key equations of this paper. They relate, respectively, the interfacial permeability, partition coefficient, and diffusion coefficient of a lipid bilayer to a given solute, relative to those of isotropic solvents, to the experimentally measurable lipid bilayer parameters, including the surface lipid density σ, the cross-sectional area of the lipid molecule a_h, and the CD-order parameter S_{CD}.

Estimation of model parameters

The predictions of Eq. 31 were tested for egg phosphatidyl choline (PC) bilayers, because a large set of permeability data exists for this model bilayer system. To use the model equations, information is required on the following parameters: the surface lipid density σ, the closed-packed area of lipids at the surface a_h, the CD-order parameter near the surface $S_{CD}^{plateau}$, the solvent hard-sphere radius R_h, the fraction of free volume in an isotropic solvent (discussed later in this section) v_f, and the solute radius r. Numerous measurements exist in the literature for σ and a_h (White and King, 1985; Kumar, 1991). The reported values of σ for egg PC bilayers is about 0.027 chains/Å^2 (corresponding to an area per lipid molecule of 73 ± 2 Å^2) (White, 1976). The closed-packed area for egg PC corresponds approximately to the area per lipid chain when the chains are tightly packed. We chose an a_h value of 25 Å^2 per lipid chain following the model of Stigter and Dill (1988). The plateau CD-order parameter value for egg PC bilayers is not available in the literature, and was assumed to be similar to that for DPPC bilayers. The reported value of the plateau CD-order parameter for DPPC bilayers is −0.2 (Xiang, 1993).

Numerous theoretical and computational studies have been performed to arrive at the appropriate hard-sphere radii R_h corresponding to various isotropic hydrocarbons. The choice of R_h depends on the choice of solvent used to represent the isotropic fluid. Since we used octanol as a model isotropic solvent (due to the availability of $K_o(r)$ values for this solvent [see Table 1]), we calculated R_h from the van der Waals volume of octane (closest hydrocarbon to octanol). We calculated the radius of the solvent molecules from their van der Waals volume assuming a spherical molecular structure. The van der Waals volume for octane was obtained from the literature (Bondi, 1964), and R_h was calculated to be 2.7 Å. The density ρ_h for octane was obtained from the International Critical Table = 0.698 gm/cc at 25°C. The fraction of free volume in octane v_f was then calculated using the relation $v_f = 1 - 4\pi R_h^3\rho_h/3$. Although the choice of R_h and ρ_h affects the magnitude of $P_b^{int}(r)/P_o(r)$, it does not affect the general characteristics of the dependence on σ, a_h, and S_{CD}. In other words, the precise choice of R_h and ρ_h does not affect the general conclusions of the model calculations.

TABLE 1 Values of molecular weights, permeabilities, octanol–water partition coefficients, molecular radii, and diffusion coefficients of several solutes

No.	Compound	Molecular Weight	Permeability (cm/s)	Partition* Coefficient ($K_{o/w}$)	Radius (Å)	$D_o \times 10^5$ (cm^2/s)	Reference
1	Water	18	3.4×10^{-3}	4.1×10^{-2}	1.6	0.72	de Gier, 1993
2	Formamide	45	7.8×10^{-5}	6.2×10^{-3}	2.1	0.54	Pozansky et al., 1975
3	Ethandiol	62	8.8×10^{-5}	1.2×10^{-2}	2.4	0.43	de Gier, 1993
4	Urea	60	4.1×10^{-6}	2.2×10^{-3}	2.3	0.46	Pozansky et al., 1976
5	Acetamide	59	2.4×10^{-5}	8.9×10^{-2}	2.3	0.46	Pozansky et al., 1976
6	Propionamide	73	6.1×10^{-5}	8.9×10^{-2}	2.5	0.4	Pozansky et al., 1976
7	Glycerol	92	5.4×10^{-6}	1.1×10^{-2}	2.7	0.35	de Gier, 1993
8	Lactic acid	90	1.4×10^{-5}	2.4×10^{-1}	2.7	0.35	Chakraborty and Deamer, 1992
9	Erythritol	122	7.5×10^{-8}	1.2×10^{-3}	3.0	0.3	de Gier, 1993
10	Glucose	180	3.0×10^{-11}	5.0×10^{-4}	3.4	0.23	Aekson and Munns, 1989
11	Tryptophan	204	4.1×10^{-10}	9.1×10^{-2}	3.5	0.24	Brunner et al., 1980
12	Phenylalanine	165	2.5×10^{-10}	3.7×10^{-2}	3.3	0.22	Brunner et al., 1980
13	Citric acid	192	3.1×10^{-11}	1.9×10^{-2}	3.5	0.24	Aekson and Munns, 1989
14	Fructose	180	4.0×10^{-10}	6.3×10^{-4}	3.4	0.23	Brunner et al., 1980

The diffusion coefficient values were estimated using the Wilke–Change equation (Perry et al. 1973). The permeabilities and octanol–water partition coefficients were obtained from the literature. The molecular radii were calculated using methods described in Estimation of Model Parameters. Note that only uncharged solutes, for which permeability and octanol–water partition coefficients are available in the literature, were included in the Table.

* Partition coefficients were obtained from corresponding references and through Hansch and Leo (1979).

The radius of the lipid chain R was calculated from a_h ($a_h = \pi R^2 \psi^{plateau}$, where $\psi^{plateau} \approx 3/2 + S_{CD}^{plateau}$). Substituting $a_h = 25$ Å^2 and $S_{CD}^{plateau} = -0.2$ yields $R = 2.48$ Å. The solute radii r were calculated from their van der Waals volumes, which were obtained from Bondi (1964). The solutes considered in our analysis include: 1, water; 2, formamide; 3, ethandiol; 4, urea; 5, acetamide; 6, propionamide; 7, glycerol; 8, lactic acid; 9, erythitol; 10, glucose; 11, tryptophan; 12, phenylalanine; 13, citric acid; and 14, fructose.

The critical free path ϵ^* was used as a fitted parameter. Fundamentally, ϵ^* depends on the method used to measure diffusion. For example, lower values of ϵ^* correspond to measurements of diffusion on a short length scale and vice versa. Different methods of measuring diffusion coefficients in lipid bilayers operate at different length scales. For example, methods such as fluorescent recovery after photobleaching measure diffusion coefficients on a length scale of microns. In contrast, methods such as quasielastic neutron scattering measure diffusion in a highly localized area (~10 nm) (Vaz and Almeida, 1991). The values of diffusion coefficients measured by these two methods vary by as much as 100-fold. This difference in the measured diffusion coefficients may be accounted for by changing the value of ϵ^*. However, at this stage, it is not possible to a priori predict the appropriate value of ϵ^*. Accordingly, we chose the value of ϵ^* that best fits the data shown in Fig. 3, *A* and *B*, in the context of our theoretical description. The ϵ^* value so deduced is 1.1 Å for trans-bilayer diffusion across egg PC bilayers. This suggests that, on average, the solute needs to jump through a distance of 1.1 Å along the bilayer normal to cross the interfacial region at a rate that explains the experimentally measured values of bilayer permeability. This value of ϵ^* is very close to the projected length of a C–C bond along the bilayer normal, L ($L = l\langle\cos\theta_k\rangle = 1.54(\frac{1}{2} - S_{CD}^{plateau}) = 1.08$ Å). Note that, because octanol may not be the best solvent model to describe isotropic solute diffusion, the implications of the determined value of ϵ^* need to be examined further.

The permeability $P_o(r)$ of an octanol layer having a thickness δ was calculated using a value of D_o calculated using the Wilke–Chang equation (Perry and Green, 1973). The value of D_o varied by a factor of about three between the smallest (water) and the largest (tryptophan) molecule examined in this study. This size-dependence of D_o is much weaker than that observed in the experimentally measured bilayer permeabilities. The octanol–water partition coefficients, $K_o(r)$, were obtained from the literature (see Table 1). The thickness of the ordered-chain region, δ, was assumed to be 5 Å (a representative thickness of the plateau region in S_{CD}). Note that solvents other than octanol could have been used in our calculations if the appropriate data (in particular, $K_o(r)$) were available, and if the chemical structure of the chosen solvent appropriately described the lipid bilayer interface. Both of these aspects about the solvent suitability are discussed extensively in the literature (Diamond and Katz, 1974; Xiang and Anderson, 1994b).

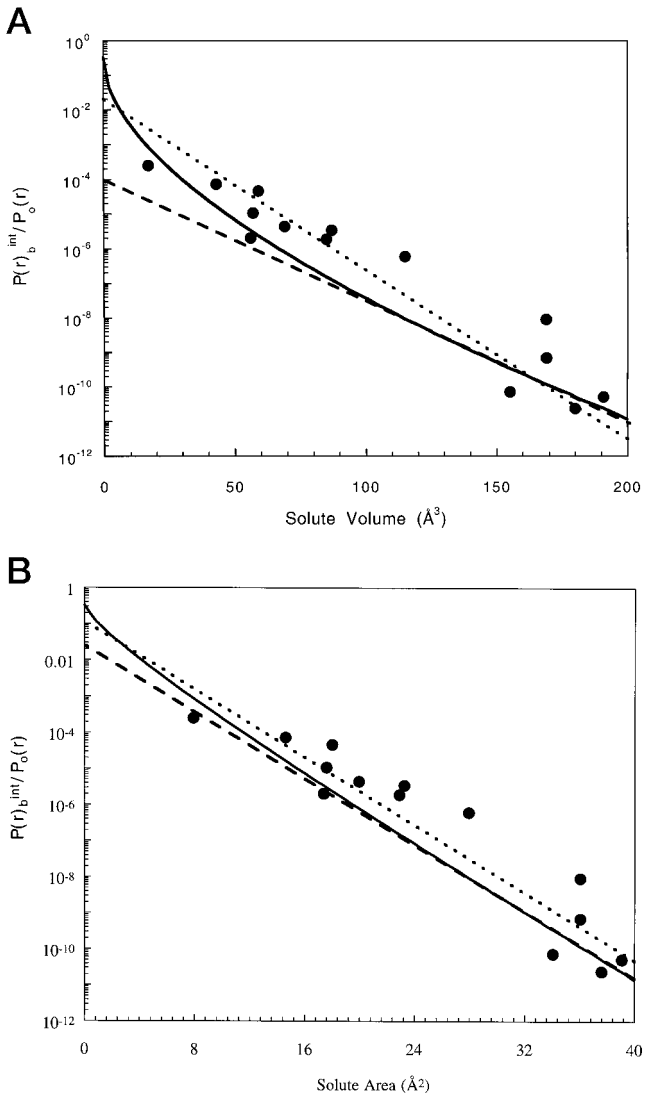

FIGURE 3 (*A*) Comparison of the predicted size dependence of the relative permeability of several solutes across unilamellar egg PC liposomes as a function of solute volume (*solid line*) with the experimentally measured values (*filled circles*, see Table 1). The model parameters used for the predictions are discussed in Estimation of Model Parameters. The *dashed line* corresponds to the trend defined by the large solutes. The *dotted line* corresponds to a single exponential fit relating relative solute permeability to solute volume. (*B*) Replot of the experimental data and theoretical predictions shown in (*A*) as a function of solute cross-sectional area. The *solid line* shows the predictions of Eq. 31. The *dashed line* corresponds to the trend defined by the large solutes. The *dotted line* corresponds to a single exponential fit relating relative solute permeability to solute cross-sectional area.

RESULTS AND DISCUSSION

Eq. 31 offers an analytical relationship for the size-dependence of the bilayer solute permeation in terms of several bilayer parameters, including surface lipid density σ, closed-packed area a_h, and CD-order parameter S_{CD}. We compared the predictions of Eq. 31 with the experimentally measured solute permeabilities across egg PC bilayers. It should be noted that, although extensive experimental data

exists for the permeation of small nonelectrolytes across lipid bilayers, care should be taken while comparing data from different studies, because experimental techniques may vary from study to study, leading to a variability in the measured values. Nonetheless, such a comparison is feasible and is reported here to assess the validity of our model. Table 1 shows a compilation of literature data for the magnitude of the permeability of various solutes across egg PC liposomes. The Table also lists literature values of van der Waals radii, molecular weights, octanol–water partition coefficients, and diffusion coefficients in octanol (predicted by the Wilke–Chang equation) for various solutes. Figure 3 *A* shows the predicted size-dependence of the interfacial (and hence, approximately bilayer) permeability, $P_b^{int}(r)/P_0(r)$, of a single egg PC bilayer based on Eq. 31 (*solid line*). The experimental permeability data is indicated by the filled circles. The model predictions compare well with the experimental observations.

Some of the previous studies of bilayer permeability have used exponential fits relating bilayer permeability to solute volume (or molecular weight) or to solute area to explain the experimentally observed permeation size-selectivity. We have, therefore, compared the predictions of Eq. 31 with such exponential fits. First, we note that the curvilinear nature of the solid line in Fig. 3 *A* clearly shows that the predictions of Eq. 31 differ from a single exponential fit relating $P_b^{int}(r)/P_0(r)$ to solute volume (which would correspond to a straight line in Fig. 3 *A*, as shown by the *dotted line*). The Figure also shows a dashed line corresponding to the trend defined by the large solutes, that is, a tangent to the solid line at a volume = 200 Å^3. Figure 3 *A* reveals that the dashed line deviates from the solid line for the small solutes (volume less than about 100 Å^3), which clearly indicates that the permeability of the small solutes is higher than that expected from the trend defined by the larger solutes. Indeed, the values of $P_b^{int}(r)/P_0(r)$ for a solute having zero volume, predicted by the solid line, dashed line, and dotted line in Fig. 3 *A*, are 0.38, $\sim 10^{-4}$, and $\sim 10^{-2}$, respectively. In general, for a zero-volume solute (that is, for a point-like solute), $P_b^{int}(r)/P_0(r)$ should be close to the ratio of free volumes in the interfacial region and in an isotropic solvent, which is 0.47 (see Eq. 31 and the free volumes described in the previous section). Therefore, $P_b^{int}(r)/P_0(r)$ for a point-like solute predicted by Eq. 31 is much closer to its expected value than that predicted by the exponential fits. Hence, while the solid line describes $P_b^{int}(r)/P_0(r)$ over the entire range of solute sizes examined in Fig. 3 *A*, the other two lines appear to grossly underpredict $P_b^{int}(r)/P_0(r)$ for the small solutes.

The deviation of the size-dependence of the experimentally measured bilayer permeability from a single exponential curve relating permeability to solute volume has indeed been reported in the past. Specifically, Walter and Gutknecht (1986) reported that solutes having molecular weights smaller than 50 (which roughly corresponds to a solute volume of $\sim$70 Å^3) permeate faster than expected based on the permeability of large (MW $>$ 50) solutes. The authors hypothesized that the extra permeability of the small solutes is related to the existence of transient aqueous pores in the bilayer, although the size and the physical basis for the existence of such pores was not clarified. Eq. 31 shows that this apparent two-region size-dependence simply results from the differential contribution of the terms appearing in this equation. Specifically, for the larger solutes, the work of cavity formation can be described by the pressure-area type work (the last term in the exponent appearing in the numerator of Eq. 31), approximately given by $\exp(-r^2)$, whereas that for smaller solutes is given by $\exp(-r)$. Since Eq. 31 predicts that the size-dependence of relatively large solutes varies as $\exp(-r^2)$, we thought that it would be informative to replot the data in Fig. 3 *A* as a function of solute cross-sectional area, rather than solute volume. This is shown in Fig. 3 *B*, where the solid line corresponds to the predictions of Eq. 31, the dashed line corresponds to the trend defined by the large solutes, which is now a straight line on a semilog plot (see Eq. 31), and the dotted line corresponds to a single exponential fit relating $P_b^{int}(r)/P_0(r)$ to solute cross-sectional area. Clearly, the three curves in Fig. 3 *B* are in much closer agreement with each other than those shown in Fig. 3 *A*. The dashed line still deviates slightly from the solid line for solute cross-sectional areas that are smaller than 15 Å^2, because the contribution of the $\exp(-r)$ term in Eq. 31 dominates for small r values. However, the theoretical predictions, as well as experimental data in Fig. 3 *B*, suggest that a single exponential fit relating $P_b^{int}(r)/P_0(r)$ to solute cross-sectional area provides a closer approximation to Eq. 31 than a single exponential fit relating $P_b^{int}(r)/P_0(r)$ to solute volume (as shown in Fig. 3 *A*). This also implies that the solute permeability across lipid bilayers should correlate better with solute cross-sectional area than with solute volume. This is clearly shown in Fig. 4, *A–C*, where the normalized relative interfacial permeability, $[P_b^{int}(r)/P_0(r)]/[P_b^{int}(r = 0)/P_0(r = 0)]$, is plotted as functions of solute radius, cross-sectional area, and volume, respectively. The various lines correspond to the best fit under the constraint that $[P_b^{int}(r)/P_0(r)]/[P_b^{int}(r = 0)/P_0(r = 0)] = 1$ when $r = 0$. Fig. 4, *A–C* shows that the overall correlation of the normalized permeability with solute cross-sectional area is much better than those with solute radius or solute volume, as judged by their correlation coefficients. A similar conclusion was reached by Xiang and Anderson (1998). The accuracy of the curve fits in Fig. 4, *A–C* can be further seen in Fig. 5, *A–C*, where the calculated residuals (the difference between the experimentally measured and predicted values using the corresponding exponential curve fits) are plotted. Figure 5 *A* shows that the residuals corresponding to the curve fit of $[P_b^{int}(r)/P_0(r)]/[P_b^{int}(r = 0)/P_0(r = 0)]$, as a function of solute radius, decrease with increasing solute radius. In contrast, the residuals corresponding to the curve fit relating $[P_b^{int}(r)/P_0(r)]/[P_b^{int}(r = 0)/P_0(r = 0)]$ to solute volume increase with increasing solute volume. A systematic error in the residuals in both cases indicates that neither represents the data fairly. In contrast, Fig. 5 *B* shows that the residuals are randomly

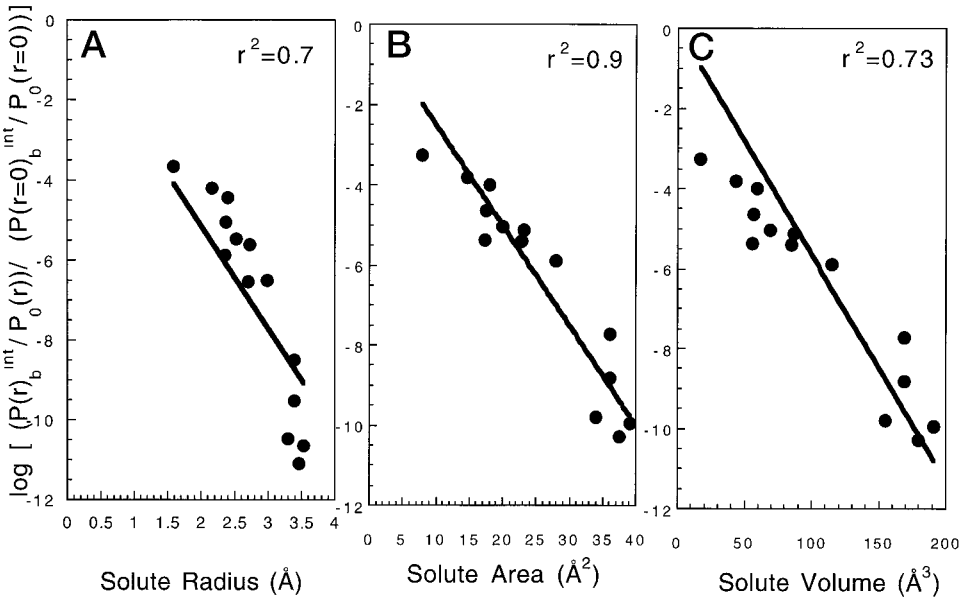

FIGURE 4 Replot of the experimental data shown in Figure 3 (normalized with respect to the solute permeability corresponding to a solute with $r = 0$ as predicted by Eq. 31, that is, $[P_b^{int}(r)/P_0(r)]/[P_b^{int}(r = 0)/P_0(r = 0)]$) as a function of (*A*) solute radius, (*B*) cross-sectional area, and (*C*) volume. The *solid lines* correspond to exponential fits of the experimental data using the equation $[P_b^{int}(r)/P_0(r)]/[P_b^{int}(r = 0)/P_0(r = 0)] = \exp(-\alpha G)$, where G is either solute radius, cross-sectional area, or volume.

distributed around zero, thus implying that an exponential fit relating $[P_b^{int}(r)/P_0(r)]/[P_b^{int}(r = 0)/P_0(r = 0)]$ to solute cross-sectional area fits the experimental data well. An interesting deviation from this conclusion involves the residual for the smallest solute in Fig. 5, *A–C* (indicated by the *arrows*) which is closer to zero in Fig. 5 *A* than in Fig. 5, *B* or *C*. This suggests that, in the case of relatively small solutes, an exponential fit relating $[P_b^{int}(r)/P_0(r)]/[P_b^{int}(r = 0)/P_0(r = 0)]$ to solute radius is more accurate than those relating it to solute cross-sectional area or solute volume. A possible explanation for this finding follows from Eq. 31, which shows that the contribution of the $\exp(-r)$ term to bilayer permeability dominates for small solutes. In other words, the work of cavity formation for relatively small solutes is proportional to the solute radius rather than to the solute cross-sectional area. Hence, it appears that, although the overall solute permeability correlates well with solute cross-sectional area, this may not hold true for small solutes. Accordingly, none of the single exponential fits examined (either with respect to solute radius, cross-sectional area, or volume) may be able to explain the experimental permeation data over a wide range of solute sizes (although the exponential fit as a function of solute cross-sectional area is better than those as a function

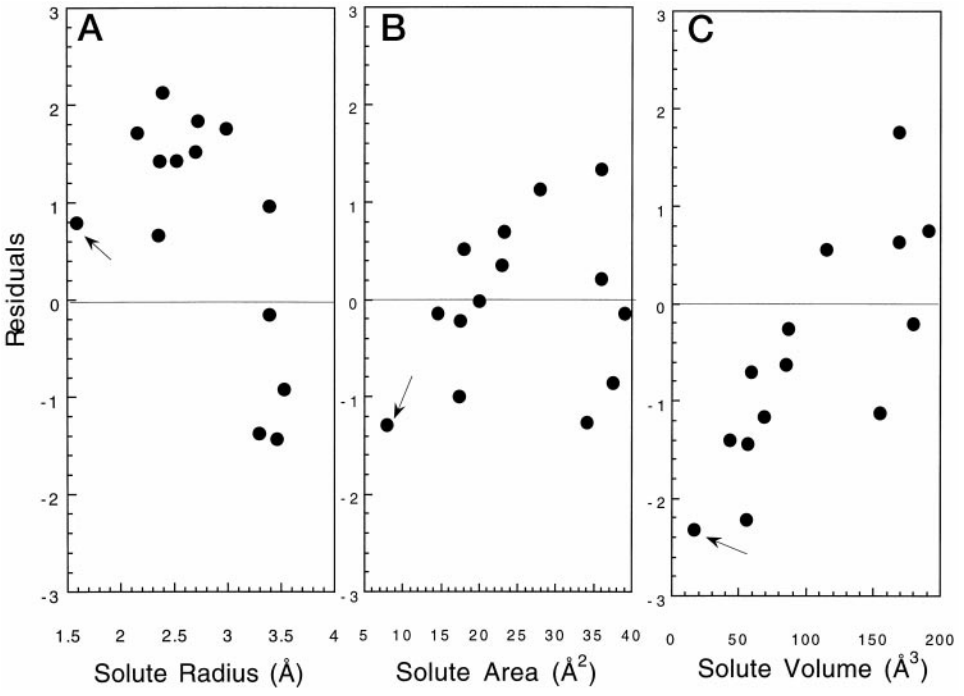

FIGURE 5 Calculated residuals (the difference between the predicted values of $[P_b^{int}(r)/P_0(r)]/[P_b^{int}(r = 0)/P_0(r = 0)]$ from the fit and the experimental values) corresponding to the data shown in Fig. 4.

of solute radius or volume). In contrast, Eq. 31, which takes into account the relationship between the work of cavity formation and solute size, is applicable over a broad solute size range.

Several attempts have been made in the past to quantitatively understand the origin of the size selectivity of bilayer permeation. The new aspect of our model is that it enables us to analytically correlate bilayer permeability to important bilayer and solute properties based on a mechanistically sound description of solute partitioning and subsequent diffusion in bilayers. A few analytical equations already exist in the literature to predict bilayer permeability. For example, an early model by Leib and Stein (1969) attributed the size dependence of bilayer permeation entirely to diffusion, based on the assumption that diffusion in a bilayer is similar to that in a polymer membrane. Although this model captured the relevant features of solute diffusion, it did not account for the contribution of partitioning to size selectivity. Recently, Xiang and Anderson (1997) proposed a free-area model to explain the permeability of acetic acid across lipid bilayers. This analytical model attributed the size dependence of bilayer permeation to partitioning and to diffusion. Their model calculated the probability for the creation of a free area for solute partitioning and diffusion across a lipid bilayer. The model implicitly assumed that the work required to create a cavity to incorporate a solute of radius r is proportional to r^2. As shown earlier, this assumption, although valid for most solutes, may underestimate the work of cavity formation required to incorporate relatively small solutes. Furthermore, their model neglected the work required to create a cavity in isotropic solvents, and may therefore lead to an overestimation of the solute size selectivity.

The predictions of our model are also in general agreement with the simulations data available in the literature. A direct comparison of the predictions of Eq. 31 with simulation data is difficult because none of the simulations report $P_b^{int}(r)/P_0(r)$. However, a comparison of the simulations data can be made with our model predictions regarding the probability of cavity formation in the interfacial region, $p^{int}(r)$ (given by Eq. 34 below, which is derived from Eq. 9 after substituting expressions for χ and ξ similar to those used in the derivation of Eq. 31). Specifically,

$$p^{int}(r) = \exp[-\beta\langle W_b(r)\rangle_{int}] = \exp\left(\ln(1-\sigma a_h) - 2\left(\frac{\sigma\sqrt{\pi a_h}}{1-\sigma a_h}\right)r - \left(\frac{\sigma\pi}{(1-\sigma a_h)^2}\right)r^2\right). \quad (34)$$

We therefore compared the values of $p^{int}(r)$ predicted from Eq. 34 with those obtained from the MD simulations of DPPC bilayers reported by Xiang and Anderson (1993). Eq. 34 indicates that two parameters, σ and a_h, are required to predict $p_{int}(r)$. The surface lipid density σ for a DPPC bilayer was chosen to be 0.033 chains/Å^2 (corresponding to a chain area of 30 Å^2/chain) (Xiang, 1993), and a_h for a DPPC bilayer was calculated from the reported free area fractions in the ordered-chain region a_f, ($a_f = 1 - \sigma a_h$) and was found to be 20.7 Å^2. Figure 6 shows a comparison of the predictions of Eq. 34 (*full line*) with the simulations (*open circles*). As can be seen, Eq. 34 predicts reasonably well the overall size-dependence of $p^{int}(r)$ for cavities formed in the ordered-chain region. The agreement of our model predictions with the simulations data is excellent for small solutes ($r < 1.54$ Å corresponding to $r^2 < 2.4$ Å^2); however, the predictions are slightly lower than the simulations values for the larger solutes ($r > 1.54$ Å). As explained earlier, the discrepancy between the predictions and the simulations for solutes having radii larger than ~1.54 Å is not surprising, because Eq. 9, on which Eq. 34 is based, is most accurate for solutes having a radius r that is smaller than the length of the lipid segment, $l = 1.54$ Å (see Calculation of $W_b(r, z)$). However, as can be seen from Fig. 6, Eq. 34 still provides a reasonable estimate of the work of cavity formation for solutes having radii greater than ~1.54 Å.

The size selectivity of bilayer partitioning, and of bilayer diffusion, depends on the surface lipid density σ, the CD-order parameter S_{CD}, and the closed-packed lipid area a_h. Note that these three parameters cannot be varied independently. Specifically, the parameters σ and S_{CD} are closely related (Nagle, 1993; De Young and K.A., 1990). Eqs. 32 and 33, respectively, provide simple, yet fundamental, relations between the solute partitioning coefficient and diffusion coefficient in the ordered-chain region and the bilayer structural characteristics. The predicted relative solute partition coefficient in the ordered-chain region, $K_b^{int}(r)/K_o(r)$, decreases with increasing surface lipid density σ. This prediction reflects the fact that the probability of cavity formation in the ordered-chain region decreases with in-

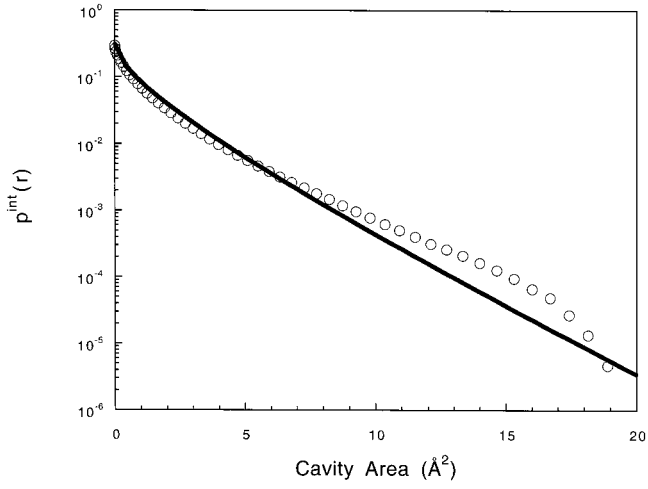

FIGURE 6 Comparison of the model predictions of $p^{int}(r)$ for various solute cross-sectional areas (*solid line* based on Eq. 34) with simulations data from the literature (Xiang, 1993) (*open circles*).

creasing lipid density. The dependence of $K_b^{int}(r)/K_o(r)$ on σ is much stronger for solutes having larger radii. Physically, this suggests that the enhancement of the probability of cavity formation due to an increase in σ is larger for the larger solutes. The dependence of the relative diffusion coefficient $D_b^{int}(r)/D_o(r)$ on σ is qualitatively similar to that of the relative partition coefficient on σ.

It is useful to quantify the relative contribution of the diffusion and the partition coefficients to size selectivity by introducing a quantity Q, defined as ($Q = [D_b^{int}(r)/D_o(r)]/[K_b^{int}(r)/K_o(r)]$. A value of $Q = 1$ indicates that hindrance to diffusion and partitioning are comparable in determining the size dependence of bilayer permeation. A value of $Q > 1$ indicates that the solute experiences more difficulty in partitioning into the ordered-chain region as compared to diffusing across it. In other words, $K_b^{int}(r)/K_o(r)$ has a larger contribution in determining the size dependence of bilayer permeation as compared to that of $D_b^{int}(r)/D_o(r)$. Figure 7 shows the predicted values of Q for the egg PC bilayer data shown in Fig. 3 as a function of solute volume. Figure 7 shows that Q may be greater or less than unity depending on solute size, thus suggesting that the relative contribution of diffusion and partitioning may vary with solute size and with other bilayer parameters. This also suggests that it is not possible to make general statements about the quantitative relative roles of diffusion and partitioning in determining the size selectivity of bilayer permeation. This is an important conclusion, because it suggests that the relative importance of partitioning and diffusion in bilayer permeation should be evaluated on a case by case basis. Although no experimental or simulations data are available to assess our model predictions for Q, the predictions regarding the relative roles of partitioning and diffusion in bilayer permeation are quite novel and could be tested by future experiments or simulations.

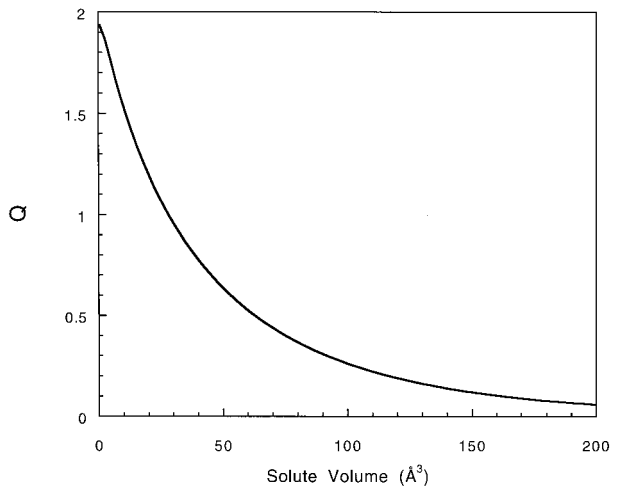

FIGURE 7 Predicted dependence of Q on solute volume at constant values of σ, 0.027 Å^{-2}; S_{CD}, −0.2; a_h, 25 Å^2; and ϵ^*, 1.1 Å.

CONCLUSIONS

The size selectivity of solute partitioning into lipid bilayers was analyzed using scaled-particle theory. A 2D scaled-particle theory description was used to calculate the reversible work required to create a circular cavity to introduce the solute into the interfacial region of the lipid bilayer. An approximate equation was derived to relate the solute partition coefficient in the ordered-chain region to three experimentally measurable bilayer parameters: the surface lipid density, the closed-packed area of the lipids, and the CD-order parameter. Additional equations were derived to describe solute diffusion in the ordered-chain region. The predicted permeabilities compare favorably with the experimentally measured bilayer permeabilities, although it should be kept in mind that specific interactions between the solute and the bilayer were not accounted for in the model presented in this paper. Finally, the extension of the theory presented here to biological systems, such as cell membranes, should be feasible, although it will require information about the structural parameters characterizing the bilayers comprising cell membranes. Nevertheless, the applicability of the general principles of bilayer permeation resulting from the trans-bilayer transport description presented in this paper may be useful in understanding transport processes in biological membranes.

APPENDIX

Consider the formation of a spherical cavity within a single layer of lipid chains in a bilayer. Since the lipid chains are modeled as a 2D system, the work of cavity formation to accommodate a spherical solute of radius r is assumed to be equal to that corresponding to the formation of a circular cavity of radius r in a plane containing elliptical cross-sections of the lipid chains. This assumption is valid for solutes having a radius r that is less than the thickness of a lipid segment. In the event that part of the solute intersects with the adjacent lipid segment, considerations of the density and ordering of the lipid segments in the adjacent chain layer are required. Note that the lipid density and lipid chain order parameters vary with depth in the lipid bilayer.

To calculate the work of cavity formation in a system of hard ellipses, an equation of state for a mixture of hard ellipses is required and is discussed first. Using scaled-particle theory, the work W_k required to introduce an ellipse k having major axis αR and minor axis λR, where α and λ are scaling parameters, in a mixture of ellipses can be obtained by generalizing the equations of Cotter (1977) for spherocylinders. Specifically,

$$\exp(-\beta W_k) = 1 - \rho \sum_{i=1}^{n} s_i S_{ik} + F_2^k(\alpha, \lambda, \rho), \quad \text{(A1)}$$

where ρ is the lipid disk density, $\beta = 1/kT$, S_{ik} is the area from which the center of ellipse k is excluded when it moves around ellipse i (having a major axis $R/\cos\theta_i$, and a minor axis R) without loosing contact with it. The first two terms in Eq. A1, that is, $1 - \rho \sum_{i=1}^{n} s_i S_{ik}$, account for the excluded-area interactions of ellipse k with all the other ellipses, whereas the third term, F_2^k, accounts for multibody interactions (Cotter, 1977). For infinitesimally small solutes (for which, $\alpha = \lambda = 0$), the terms accounting for multibody interactions must vanish, that is,

$$(F_2^k)_{\alpha=\lambda=0} = \left(\frac{\partial F_2^k}{\partial \alpha}\right)_{\alpha=\lambda=0} = \left(\frac{\partial F_2^k}{\partial \lambda}\right)_{\alpha=\lambda=0} = 0$$

(Cotter, 1977). In contrast, for infinitely large solutes (for which $\alpha = \lambda = \infty$), W_k must reduce to a pressure-area type work. These considerations suggest that W_k may be described approximately by the equation (Cotter, 1977),

$$\beta W_k = C_{00} + C_{10}\alpha + C_{01}\lambda + \alpha\lambda R^2\beta P, \qquad \text{(A2)}$$

where P is the 2D pressure, and the coefficients C_{lm} can be described by (Cotter, 1977)

$$C_{lm} = (l!\ m!)^{-1}\left(\frac{\partial^{(l+m)}W_k}{\partial\alpha^l\partial\lambda^m}\right)_{\alpha=\lambda=0}. \qquad \text{(A3)}$$

These coefficients can be calculated by substituting Eq. A2 in Eq. A1 after a formal expression for S_{ik} is known. Because F_2^k, as well as its derivatives, vanish at $\alpha = \lambda = 0$, the actual evaluation of F_2^k is not necessary. The central quantity of interest is S_{ik}, the area from which the center of ellipse i is excluded by ellipse k. S_{ik} was calculated using an approach similar to that of Boublik (1974). Consider two ellipses, i and k, having areas S_i and S_k and perimeters L_i and L_k. S_{ik} (averaged over all the orientations of k with respect to i) can be obtained following the approach developed by Kihara (1963). Specifically,

$$S_{ik} = S_i + S_k + \frac{L_iL_k}{2\pi}. \qquad \text{(A4)}$$

Hence, the excluded area when an ellipse k having a major axis αR and a minor axis λR is introduced into a system consisting of ellipses i, each having an area S_i, and perimeter L_i, is given by (noting that $L_k = 2\pi R\sqrt{(\alpha^2 + \lambda^2)/2}$ and $S_k = \pi R^2\alpha\lambda$)

$$S_{ik} = S_i + \pi R^2\alpha\lambda + L_iR\sqrt{(\alpha^2 + \lambda^2)/2}. \qquad \text{(A5)}$$

Substituting Eq. A5 in Eq. A1, and then substituting the resulting expression in Eq. A3, the coefficients C_{lm} can be evaluated. Substituting the resulting values of C_{lm} in Eq. A2 then yields

$$\beta W_k = -\ln\left(1 - \rho\sum_i s_iS_i\right) + \frac{(\rho/2)\sum_i s_iL_i}{(1 - \rho\sum_i s_iS_i)}(\alpha R + \lambda R) + \pi\alpha\lambda R^2\beta P. \qquad \text{(A6)}$$

Therefore, the work required to introduce an ellipse of major axis $R/\cos\theta_k$, and minor axis R is obtained by substituting $\lambda = 1$ and $\alpha = 1/\cos\theta_k$ in Eq. A6, including substituting analytical expressions for the area, $S_i = \pi R^2/\cos\theta_i$, and perimeter $L_i = 2\pi R\sqrt{½ + 1/(2\cos^2\theta_i)}$, of ellipse i. In that case, Eq. A6 reduces to

$$\beta W_k = -\ln\left(1 - \rho\pi R^2\sum_i\frac{s_i}{\cos\theta_i}\right) + \frac{\pi\rho R^2\sum_i s_i\sqrt{½[1 + (1/\cos^2\theta_i)]}}{[1 - \rho\pi R^2\sum_i(s_i/\cos\theta_i)]}\left(\frac{1}{\cos\theta_k} + 1\right) + \frac{\pi R^2}{\cos\theta_k}\beta P. \qquad \text{(A7)}$$

The pressure, P, can now be calculated using the relation, $(\partial P/\partial\rho)_{s_1,s_2\ldots} = 1 + \rho(\partial\bar{W}/\partial\rho)_{s_1,s_2\ldots}$ (Cotter, 1977), where $\bar{W} = \Sigma_k W_k$. The resulting equation of state for a mixture of hard ellipses is then given by

$$\beta P = \frac{1}{\pi R^2\psi}\left(\frac{1 - \xi/\psi}{1 - \rho\pi R^2\psi} + \frac{\xi/\psi}{2(1 - \rho\pi R^2\psi)^2} + \frac{\xi}{2\psi} - 1\right), \qquad \text{(A8)}$$

where

$$\psi = \sum_{k=1}^{N}\frac{s_k}{\cos\theta_k}$$

and

$$\xi = (1 + \psi)\sum_{k=1}^{N}s_k\sqrt{\frac{1}{2}\left(1 + \frac{1}{\cos^2\theta_k}\right)}.$$

Eq. A8 indicates that the pressure of a multicomponent hard-ellipse system depends on three parameters: the density ρ, minor axis R, and the parameters related to the eccentricity ψ and ξ. Note that Eq. A8 reduces to the well-known equation of state for hard circular disks (Helfand et al., 1961) after substituting $\psi = 1$ and $\xi = 2$.

The work required to introduce a spherical solute of radius r in the ordered-chain region, $W_b(r, z)$, can be calculated by substituting $\alpha = \lambda = r/R$ in Eq. A6, and using Eq. A8 to describe the pressure P along with substituting analytical expressions for the area, $S_i = \pi R^2/\cos\theta_i$, and perimeter $L_i = 2\pi R\sqrt{½ + 1/(2\cos^2\theta_i)}$, of ellipse i, and representing the summations by ψ and ξ as shown above. The resulting expression is given in Eq. 9 in the main text.

We are grateful to Professor Tian-Xiang Xiang for providing his simulation data. This work was supported by a National Institutes of Health grant #GM 44884.

REFERENCES

Aekson, M., and D. Munns. 1989. Lipid bilayer permeation by neutral aluminum citrate and by three α-hydroxy carboxylic acids. *Biochim. Biophys. Acta.* 984:200–206.

Bondi, A. 1964. Van der Waals volumes and radii. *J. Phys. Chem.* 68: 441–451.

Boublik, T. 1974. Statistical thermodynamics of convex molecule fluid. *Mol. Phys.* 27:1415–1427.

Brunner, D., D. Graham, H. Hauser, and G. Semenza. 1980. Ion and sugar permeabilities of lecithin bilayers: comparison of curved and planar bilayers. *J. Membr. Biol.* 57:133–141.

Chakraborty, A., and D. W. Deamer. 1992. Permeability of lipid bilayers to amino acids and phosphates. *Biochim. Biophys. Acta.* 1111:171–177.

Cotter, M. A. 1977. Hard spherocylinders in an anisotropic mean field: a simple model for a nematic liquid crystal. *J. Chem. Phys.* 66: 1098–1106.

de Gier, J. 1993. Osmotic behavior and permeability properties of liposomes. *Chem. Phys. Lip.* 64:187–196.

De Young, L. R., and K. A. Dill. 1990. Partitioning of non-polar solutes into bilayers and amorphous *n*-alkanes. *J. Phys. Chem.* 94:801–809.

Diamond, J. M., and Y. Katz. 1974. Interpretation of nonelectrolyte partition coefficients between lecithin and water. *J. Membr. Biol.* 17: 121–154.

Dix, J. A., D. Kivelson, and J. M. Diamond. 1978. Molecular motion of small non-electrolyte molecules in lecithin bilayers. *J. Membr. Biol.* 40:315–342.

Han, J., and J. Herzfeld. 1993. Macromolecular diffusion in crowded solution. *Biophys. J.* 65:1155–1161.

Hansch, C., and A. Leo. 1979. Substituent Constants for Correlation Analysis in Chemistry and Biological Sciences. Wiley. New York.

Helfand, E., H. L. Frisch, and J. L. Lebowitz. 1961. Theory of the two- and one-dimensional rigid spheres. *J. Chem. Phys.* 34:1037–1042.

Huang, P., J. J. Perez, and G. H. Loew. 1994. Molecular dynamics simulations of phospholipid bilayers. *J. Biomol. Struct. Dyn.* 11: 927–956.

Hummer, G., S. Garde, A. E. Garcia, A. Pohorille, and L. R. Pratt. 1996. An information theory model of hydrophobic interactions. *Proc. Natl. Acad. Sci. USA.* 93:8951–8955.

Jansson, M. J., R. L. Thurmond, J. A. Barry, and M. F. Brown. 1992. Deuterium NMR study of intermolecular interactions in lamellar phases containing palmitoylysophosphatidylcholine. *J. Phys. Chem.* 96: 9532–9544.

Johnson, M. E. 1996. Biophysical aspects of transdermal drug delivery and chemical enhancement. Ph.D. thesis. Massachusetts Institute of Technology, Cambridge.

Kihara, T. 1963. Convex molecules in gaseous and crystalline states. *Adv. Chem. Phys.* 5:147.

Kumar, V. V. 1991. Complementary molecular shapes and additivity of the packing parameters of lipids. *Proc. Natl. Acad. Sci. USA.* 88:444–448.

Lebowitz, J. L., E. Helfand, and E. Praestgaard. 1965. Scaled particle theory of fluid mixtures. *J. Chem. Phys.* 43:774–779.

Leib, W. R., and W. D. Stein. 1969. Biological membranes behave as non-porous polymeric sheets with respect to the diffusion of non-electrolytes. *Nature.* 224:240–243.

Marqusee, J. A., and K. A. Dill. 1986. Solute partitioning into chain molecule interphases: monolayers, bilayer membranes, and micelles. *J. Chem. Phys.* 85:434–444.

Marrink, S. J., and H. J. C. Berendsen. 1994. Simulation of water transport through a lipid membrane. *J. Phys. Chem.* 98:4115–4168.

Marrink, S. J., and J. C. Berendsen. 1996. Permeation process of small molecules cross lipid membranes studies by molecular dynamics simulations. *J. Phys. Chem.* 100:16729–16738.

Nagle, J. F. 1993. Area lipid of bilayer from NMR. *Biophys. J.* 64: 1476–1481.

Perry, R. H., and D. W. Green. 1973. Chemical Engineers Handbook. McGraw-Hill Book Company, New York. 5–51.

Pozansky, J., S. Tong, P. C. White, J. M. Mil-Gram, and A. K. Solomon. 1976. Nonelectrolyte diffusion across lipid bilayer systems. *J. Gen. Physiol.* 67:45–66.

Reiss, H., H. L. Frisch, and J. Lebowitz. 1959. Statistical mechanics of rigid spheres. *J. Chem. Phys.* 31:369–380.

Salmon, A., S. W. Dodd, G. D. Williams, J. M. Beach, and M. F. Brown. 1987. Configurational statistics of acyl chains in polyunsaturated lipid bilayers from 2H NMR. *J. Am. Chem. Soc.* 109:2600–2609.

Seeling, A., and J. Seeling. 1974. The dynamics structure of fatty acyl chains in a phospholipid bilayer measured by deuterium magnetic resonance. *Biochemistry.* 13:4839–4845.

Stein, W. D. 1986. Diffusion and Transport across Cell Membranes. Academic Press, Orlando, FL.

Stigter, D., and K. Dill. 1988. Lateral interactions among phospholipid head groups at the heptane/water interface. *Langmuir.* 4:200–209.

Vaz, W. L. C., and P. F. Almeida. 1991. Microscopic versus macroscopic diffusion in one-component fluid phase lipid bilayer membranes. *Biophys. J.* 60:1553–1554.

Vaz, W. L. C., R. M. Clegg, and D. Hallmann. 1985. Translational diffusion in lipids in liquid crystalline phase phosphatidylcholine multibilayers. A comparison of experiment with theory. *Biochemistry.* 26:781–786.

Walter, A., and J. Gutknecht. 1986. Permeability of small nonelectrolytes through lipid bilayer membranes. *J. Membr. Biol.* 90:207–217.

White, S. 1976. The lipid bilayer as a solvent for small hydrophobic molecules. *Nature.* 262:421–422.

White, S. H., and G. I. King. 1985. Molecular packing and area compressibility of lipid bilayers. *Proc. Natl. Acad. Sci. USA.* 82:6532–6536.

White, S. H., G. I. King, and J. E. Cain. 1981. Location of hexane in lipid bilayers determined by neutron diffraction. *Nature (Lond.).* 290: 161–163.

Xiang, T.-X. 1993. A computer simulation of free-volume distributions and related structural properties in a model bilayer. *Biophys. J.* 65: 1108–1120.

Xiang, T.-X., and B. Anderson. 1998. Influence of chain ordering on the selectivity of dipalmitoylphosphatidylcholine bilayer membranes for permeant size and shape. *Biophys. J.* 75:2658–2671.

Xiang, T.-X., and B. D. Anderson. 1993. Molecular distribution in interphases: statistical mechanical theory combined with molecular dynamics simulation of a model bilayer. *Biophys. J.* 66:561–572.

Xiang, T.-X., and B. D. Anderson. 1994a. The relationship between permeant size and permeability in lipid bilayer membranes. *J. Membr. Biol.* 140:111–121.

Xiang, T.-X., and B. D. Anderson. 1994b. Substituent contributions to the permeability of substituted p-toluic acids in lipid bilayer membranes. *J. Pharm. Sci.* 83:1511–1518.

Xiang, T.-X., and B. D. Anderson. 1997. Permeability of acetic acid across gel and liquid-crystalline lipid bilayers conforms to free-surface-area theory. *Biophys. J.* 72:223–237.

Xiang, T. X. 1999. Translational diffusion in lipid bilayers: dynamic free-volume and molecular dynamics simulation. *J. Phys. Chem.* 103: 385–394.